Mapping the uncertainty in global CCN using emulation

LEE, L.A. <http://orcid.org/0000-0002-8029-6328>, CARSLAW, K.S., PRINGLE, K.J. and MANN, G.W.

Atmos. Chem. Phys., 12, 9739–9751, 2012
www.atmos-chem-phys.net/12/9739/2012/
doi:10.5194/acp-12-9739-2012

Atmospheric Chemistry and Physics

Mapping the uncertainty in global CCN using emulation

L. A. Lee, K. S. Carslaw, K. J. Pringle, and G. W. Mann

Institute for Climate and Atmospheric Science, School of Earth and Environment, University of Leeds, UK

Correspondence to: L. A. Lee (l.a.lee@leeds.ac.uk)

Received: 11 April 2012 – Published in Atmos. Chem. Phys. Discuss.: 6 June 2012
Revised: 19 September 2012 – Accepted: 1 October 2012 – Published: 25 October 2012

Abstract. In the last two IPCC assessments aerosol radiative forcings have been given the largest uncertainty range of all forcing agents assessed. This forcing range is really a diversity of simulated forcings in different models. An essential step towards reducing model uncertainty is to quantify and attribute the sources of uncertainty at the process level. Here, we use statistical emulation techniques to quantify uncertainty in simulated concentrations of July-mean cloud condensation nuclei (CCN) from a complex global aerosol microphysics model. CCN was chosen because it is the aerosol property that controls cloud drop concentrations, and therefore the aerosol indirect radiative forcing effect. We use Gaussian process emulation to perform a full variance-based sensitivity analysis and quantify, for each model grid box, the uncertainty in simulated CCN that results from 8 uncertain model parameters. We produce global maps of absolute and relative CCN sensitivities to the 8 model parameter ranges and derive probability density functions for simulated CCN. The approach also allows us to include the uncertainty from interactions between these parameters, which cannot be quantified in traditional one-at-a-time sensitivity tests. The key findings from our analysis are that model CCN in polluted regions and the Southern Ocean are mostly only sensitive to uncertainties in emissions parameters but in all other regions CCN uncertainty is driven almost exclusively by uncertainties in parameters associated with model processes. For example, in marine regions between 30° S and 30° N model CCN uncertainty is driven mainly by parameters associated with cloud-processing of Aitken-sized particles whereas in polar regions uncertainties in scavenging parameters dominate. In these two regions a single parameter dominates but in other regions up to 50 % of the variance can be due to interaction effects between different parameters. Our analysis provides direct quantification of the reduction in variance that would result if a parameter could be specified precisely. When extended to all process parameters the approach presented here will therefore provide a clear global picture of how improved knowledge of aerosol processes would translate into reduced model uncertainty.

1 Introduction

Many of the atmospheric processes that control and shape the global aerosol distribution cannot be explicitly treated in models, either due to a lack of understanding or through computational constraints. Treatment of these processes in models thus relies on simplified parameterisations, which often contain parameters that are not well constrained by measurements or theory. This parametric uncertainty means that every model simulation has some degree of uncertainty associated with it. Although one-at-a-time sensitivity tests are commonly used to estimate the range of model predictions, these are far from adequate for estimating the associated confidence interval around the model since no parameter interactions can be taken into account. Rather, most effort to define uncertainty has focused on multi-model inter-comparisons (Schimel et al., 1996; Penner et al., 2001; Forster et al., 2007; Textor et al., 2006, 2007; Meehl et al., 2007), which provide an important insight into model diversity, but no estimate of the parametric uncertainty of the individual models. In our study, we focus on parameter uncertainty in a single model, quantifying and attributing uncertainties in simulated CCN concentrations from several uncertain model parameters.

Sensitivity analysis (SA) offers a way of quantifying model uncertainty and identifying which processes contribute most to it. SA is usually carried out using standard "one-at-a-time" (OAT) sensitivity tests which systematically investigate departures of model behaviour from some baseline. However, OAT tests cannot identify and quantify

interactions between parameters and they consider only a small fraction of the total parameter uncertainty space (Saltelli and Annonia, 2010). A more comprehensive approach is to use Monte Carlo simulations in which the statistical distribution of the model output is populated by sampling thousands of possible parameter values across the multi-dimensional parameter uncertainty space. The output distribution is then used for the sensitivity analysis, such as analysis of variance and variance decomposition to understand contributions to the overall variance. However, Monte Carlo simulation requires a very large number of model simulations, which is normally prohibitively expensive for complex atmospheric models.

A number of studies have been carried out to assess parameter uncertainty in aerosol models. Pan et al. (1997) used probabilistic collocation to represent the computer model and carry out uncertainty analysis of the aerosol indirect effect. Ackerley et al. (2009) used a general circulation model (GCM) to study the uncertainty in parameters determining atmospheric aerosol and its effect on the climate. Haerter et al. (2009) and Lohmann and Ferrachat (2010) used the ECHAM global model to study the parametric uncertainty in aerosol and its effect on clouds but in both cases the number of parameters studied was limited by the method. Haerter et al. (2009) studied the effect of perturbations of 7 cloud-related parameters on the aerosol indirect effect with interactions identified by the differences between OAT experiments and multiple parameter perturbation experiments. Lohmann and Ferrachat (2010) used a factorial design with 4 parameters to examine the effect of parametric uncertainty on clouds. Partridge et al. (2012) apply Markov Chain Monte Carlo (MCMC) methods to a cloud parcel model to investigate cloud-aerosol sensitivity to parameter uncertainty. In this study we illustrate the method of emulation to make statistical inferences about the relative effect of aerosol parameter uncertainties and their interactions on the cloud-related quantity CCN with 8 parameters using a sophisticated aerosol model. This method can easily be extended to more model parameters and outputs as well as different models.

We use emulation to carry out a parametric sensitivity analysis of a global aerosol model. An emulator is a statistical interpolator which takes the output of model simulations spread throughout the parameter uncertainty space and estimates the output throughout the rest of the space using conditional probability theory. We describe the methodology of emulation in detail in Lee et al. (2011) (hereafter Lee11) where we presented the first application of Gaussian process emulation for sensitivity analysis of a global aerosol model. The results presented in this work use the same GLOMAP simulations as presented in Lee11 and vary the same 8 uncertain parameters (detailed below), but in this work we use different computational software to enable analysis of every model gridbox to provide global maps (Lee11 was restricted to analysis of two gridboxes). As with Lee11 we emulate the simulated CCN concentration, the subset of the aerosol population that can form cloud droplets. This is a key quantity in the prediction of the aerosol indirect effect. The advantage of extending the analysis from point locations to the global scale is clear: it allows the identification of regions where parametric uncertainty strongly affects CCN and identifies the role of the different parameters in different regions.

2 Aerosol model description

The GLObal Model of Aerosol Processes (GLOMAP-mode) (Mann et al., 2010) simulates the size distribution and composition of a population of aerosol particles. The model includes new particle formation, coagulation, gas-to-particle transfer and cloud processing. GLOMAP-mode treats the aerosol size distribution using 7 lognormal modes (soluble nucleation, Aitken, accumulation and coarse modes plus water-insoluble Aitken, accumulation and coarse modes for initially insoluble soot and dust particles). The modes describe the functional shape of the particle size distribution (particle number versus size). Such a modal model provides a simpler and more computationally efficient representation of the particle distribution than alternative sectional schemes in which the particle distribution is described as a number versus size histogram (Spracklen, 2005; Mann et al., 2012). The model physical and chemical processes calculate the time dependent evolution and interaction of the number concentration and size of particles within the seven modes. GLOMAP-mode is implemented within the TOMCAT global 3-D offline chemistry transport model (Chipperfield, 2006), which has a spatial resolution of $2.81 \times 2.81^{\circ}$ and 31 vertical levels. The model is run with the same setup as described in detail by (Mann et al., 2010). It includes sea spray, black carbon, organic carbon and dust and has been shown to compare well with ground based observations of aerosol mass and number (Mann et al., 2010; Spracklen et al., 2010).

The GLOMAP-mode aerosol model is significantly more complex in its design than the models used in climate simulations. The main difference is that GLOMAP-mode simulates the evolution of the aerosol size distribution, while climate models typically simulate only the masses of the aerosol chemical components or assume a fixed size distribution. Thus, GLOMAP-mode requires many more parameters to describe the particle distribution as well as parameters defining the microphysical processes that control size-dependent particle growth, formation, coagulation, deposition, etc.

The model was spun up for three months before any parameter perturbation was applied. After perturbation, a further 3 months of spin up was permitted and the analysis was done on the fourth month after perturbation, in this case July 2000. At the resolution used here GLOMAP-mode takes about 1.4 h to run per month on 32 cores.

3 Statistical methods

The experimental design and emulator validation are outlined in detail in Lee11, but for clarity we recap some of the methodology here.

The emulation used here is a non-parametric technique based on the well-established statistical theory of the Gaussian process (O'Hagan, 2006). Gaussian process emulation is a Bayesian technique in which the prior probability distribution of the GLOMAP output is conditioned on some model-simulated output to produce a posterior probability distribution for the output. With the (unknown) July CCN defined by Y, the uncertain parameters defined by $\boldsymbol{X} = \{X_1, \ldots, X_8\}$ and GLOMAP defined as the function η we have $Y = \eta(\boldsymbol{X})$. The model simulated output (training data) is $y_1 = \eta(\boldsymbol{x}_1), \ldots, y_{80} = \eta(\boldsymbol{x}_{80})$. We use emulation to estimate η by $\hat{\eta}$ and use this to perform the sensitivity analysis. The prior distribution is the Gaussian process with mean

$$m(\boldsymbol{x}) = h(\boldsymbol{x})^{\mathrm{T}}\boldsymbol{\beta}$$

where $h(\cdot)$ is a known function of $\boldsymbol{x}$ with unknown coefficients $\boldsymbol{\beta}$. In this work $h(\cdot)$ is the simple linear regression function and the coefficients calculated using the training data. The prior covariance function is

$$\mathrm{cov}(\boldsymbol{x}, \boldsymbol{x}') = \sigma^2 c(\boldsymbol{x}, \boldsymbol{x}')$$

where $c(\boldsymbol{x}, \boldsymbol{x}') = \exp\{-\Sigma_{i=1}^{8}\left(\frac{(x_i - x_i')}{\delta_i}\right)^2\}$ is the Gaussian correlation function depending on the distance between pairs of points and the smoothness of the model response to each parameter defined by $\boldsymbol{\delta}$ calculated from the training data. The prior distributions here are typically used as uninformative priors for the Gaussian process, so in effect all posterior information comes from the training data. It is possible once the model runs are available to build the emulator with different prior assumptions. Here, the emulator was built with different covariance functions and different input distributions with little difference in the results.

The resulting emulator is a conditional probability distribution for η representing the behaviour of a given GLOMAP output given the chosen inputs with mean

$$m^*(\boldsymbol{x}) = h(\boldsymbol{x})^{\mathrm{T}}\hat{\boldsymbol{\beta}} + t(\boldsymbol{x})^{\mathrm{T}}A^{-1}(y - H\hat{\boldsymbol{\beta}})$$

and covariance matrix

$$\mathrm{cov}^*(\boldsymbol{x}, \boldsymbol{x}') = \sigma^2[c(\boldsymbol{x}, \boldsymbol{x}') - t(\boldsymbol{x})^{\mathrm{T}}A^{-1}t(\boldsymbol{x}') + (h(\boldsymbol{x}) - t(\boldsymbol{x})^{\mathrm{T}}A^{-1}H)(H^{\mathrm{T}}A^{-1}H)^{-1}(h(\boldsymbol{x}') - t(\boldsymbol{x}')^{\mathrm{T}}A^{-1}H)^{\mathrm{T}}].$$

The details of these equations can be found in Lee11. The emulator provides an estimate of the model output at any previously untried point $\boldsymbol{x}$ in the parameter uncertainty space with uncertainty; the emulator passes through every point in the training data with no uncertainty and uncertainty increases as the distance from the training data increases. The more information from model simulations that is used to produce the emulator the smaller the emulator uncertainty will be, so the reduction in uncertainty due to emulation has to be balanced with the increased efficiency from using emulation rather than direct simulation. The emulator is validated by comparing emulator predictions and its uncertainty, $m^*(\boldsymbol{x}) \pm 2 \times \sqrt{\mathrm{cov}^*(\boldsymbol{x}, \boldsymbol{x})}$, to actual GLOMAP output, $\eta(\boldsymbol{x})$, at some previously untried parameter settings $\boldsymbol{x}$ (see Lee11). The validation will reveal any issues with the choice of prior distribution, in particular the covariance function and the smoothness of the model response. If the emulator is not validated according to some acceptance criteria then the prior assumptions can be changed or more training data obtained and the emulator rebuilt. The emulator will not be validated if there are regions of sharp change in the model response to changes in parameters (i.e., the model is not smooth). The validation will show where the discontinuities in the model response lie, providing valuable information on the model behaviour. In such cases other methods of representing the model response for sensitivity analysis will have to be considered. This was not the case in our study. If the emulator is deemed valid according to some defined critical level then the areas of parameter space that were not covered by the GLOMAP simulations can be investigated using the emulator with no need for further model simulations. The defined critical level is usually 5 % (leading to a 95 % confidence level for the emulation uncertainty intervals) but can be defined by the user. The sensitivity analysis is then carried out using the emulator mean $m^*(\boldsymbol{x})$ conditioned on GLOMAP. In this work, separate emulators are built for each monthly mean CCN value in every grid box on one vertical level of the model, which amounts to 8192 emulators. The sensitivity analysis is carried out carried out in every model grid box taking no account of the spatial correlation.

The sensitivity analysis used here is the extended-FAST (Fourier Amplitude Sensitivity Test) method (Saltelli et al., 1999) which calculates two measures of sensitivity based on the variance of $m^*(\boldsymbol{x})$ after sampling $\boldsymbol{x}$ from the 8-dimensional uncertainty space:

> *The main effect* measures the reduction in the output variance if the parameter could be learnt exactly. This is the output sensitivity to each parameter alone.
>
> *The total effect* measures the reduction in the output variance when everything but the parameter is learnt. This is the output sensitivity to each parameter and its interactions.

The emulator is built using the statistical software R (R Development Core Team, 2011) with the package DiceKriging (Roustant et al., 2011) and sensitivity analysis is carried out using the package sensitivity (Pujol, 2008). The Latin hypercube sampling is carried out using the package lhs (Carnell, 2009).

The sensitivity analysis here focuses on the scalar monthly mean CCN concentration on the 915 hPa altitude level of the model and quantifies its sensitivity to 8 model parameters. This model level was chosen because this is around the altitude of cloud base and therefore the impact of changes in CCN will be relevant for the radiative properties of clouds and the indirect forcing. The 8 model parameters were identified in a previous model sensitivity study Spracklen et al. (2005) as potentially important. We recognise that 8 parameters is only a subset of the total parameter uncertainty but here we demonstrate the technique of emulation of CCN on a global scale for the first time. As in Lee11 no formal elicitation was done. The parameters and their uncertainty limits are summarised in Table 1. Eighty model runs were used to train the emulator, with points in 8-dimensional parameter space defined by a Latin-Hypercube maximin algorithm (McKay et al., 1979). The simulations took 351 h on 32 cores, or nearly 15×32 core-days. The same 80 model runs were used in Lee11. In a follow-up study we have identified 37 uncertain parameter and are investigating the uncertainty in CCN and other model outputs to 28 of these parameters after expert elicitation allowing further process representations (such as nucleation and dry deposition) to be included in the analysis; here we use only 8 to illustrate the method more clearly.

4 Results

4.1 Emulator validation

As in Lee11 emulation can only be used for sensitivity analysis in every grid box if it is validated according to some criteria. In Lee11 the validation was simple since there were only two emulators to validate (one for each grid box). Here we have 8192 emulators to validate. The validation procedure is the same as in Lee11 whereby extra runs of GLOMAP are compared to the emulator predictions but a summary of the results is required. The first summary result does not involve these extra GLOMAP runs but quantifies the uncertainty around the emulator predicted mean due to the emulation as which is done analytically in Lee11 using GEM-SA (Kennedy, 2004). The uncertainty around the emulator predicted mean output in every grid box has to be small compared to the uncertainty around the emulator mean output due to the uncertain parameters (in Lee11 these values are defined as $V^*(E)$ and $E^*(V)$). In the DiceKriging package the emulator uncertainty has to be simulated. The posterior mean function is used to carry out the sensitivity analysis but there are infinitely many possible functions within the emulator uncertainty which we can simulate and compare to obtain an estimate of the emulator uncertainty. For the 14 grid boxes shown in Fig. 2 the simulated uncertainty around the emulator mean due to the emulation ($V^*(E)$) and due to the uncertain parameters ($E^*(V)$) is shown in Table 2 (to show that these values are a result of simulation rather than analytically calculated they are defined by $\hat{V}^*(E)$ and $\hat{E}^*(V)$ here). The values in Table 2 are calculated by simulating 1000 possible functions from the posterior Gaussian process conditioned on the training data. Table 2 shows that for the 14 grid boxes in Fig. 2 the uncertainty around the emulator estimated July CCN is small compared to the uncertainty due to the uncertain parameters and so the signal to noise ratio of the function is large enough to get a meaningful sensitivity analysis. For comparison the same results were obtained by GEM-SA showing consistency in the results. As in Lee11 the emulator prediction and its uncertainty can be plotted versus the GLOMAP prediction and investigated. Figure 1a shows an example of the grid box validation. It should be noted here that 3 of the original validation runs in Lee11 were removed as their input settings were incorrect in the GLOMAP run. The validation plot shown in Fig. 1a is summarised for every grid box in Fig. 1b by counting how many of the emulator uncertainty intervals contain the GLOMAP prediction. Figure 1b shows some regions where the emulator uncertainty does not contain the GLOMAP prediction at least 90 % of the time, further investigation of these regions shows that the emulator prediction and the GLOMAP prediction are in fact very close but the emulator is too confident and so the interval too small. An example of regions where the emulator is too confident but is nonetheless doing a good job of predicting the GLOMAP value is shown in Fig. 1c. In this case it is clear that the validation points close to the training data do not match the GLOMAP run and contain small bias indicating that σ^2 is underestimated here. In such cases the emulator prior assumptions can be changed to increase the emulator uncertainty but in this case this would not improve the sensitivity analysis which depends only on the mean values (marked by dots in Fig. 1a and c). Diagnostic plots are also created by DiceKriging but as with the in-built diagnostics in GEM-SA the validation is not out-of-sample, despite this the diagnostics available in DiceKriging and GEM-SA (GEM-SA is only checked for the 14 grid boxes in Table 2) were checked and show no reason to declare the emulators used here invalid. Given all the results together in Table 2, Fig. 1 and the software diagnostic checks we declare our emulators valid for purpose and carry out sensitivity analysis for every grid box using its associated emulator.

4.2 CCN parametric uncertainty

Figure 2 shows the emulated mean CCN and standard deviation in every surface grid box resulting from uncertainty in the 8 model parameters as described above. Also shown for comparison is the mean CCN from the 80 GLOMAP simulations in the experimental design. Results are shown for July 2000. Figure 2 shows that emulated mean CCN concentrations are very close to the mean simulated CCN, as expected given the uniform input parameter uncertainty distributions used here and a sufficient experimental design. Figure 2c

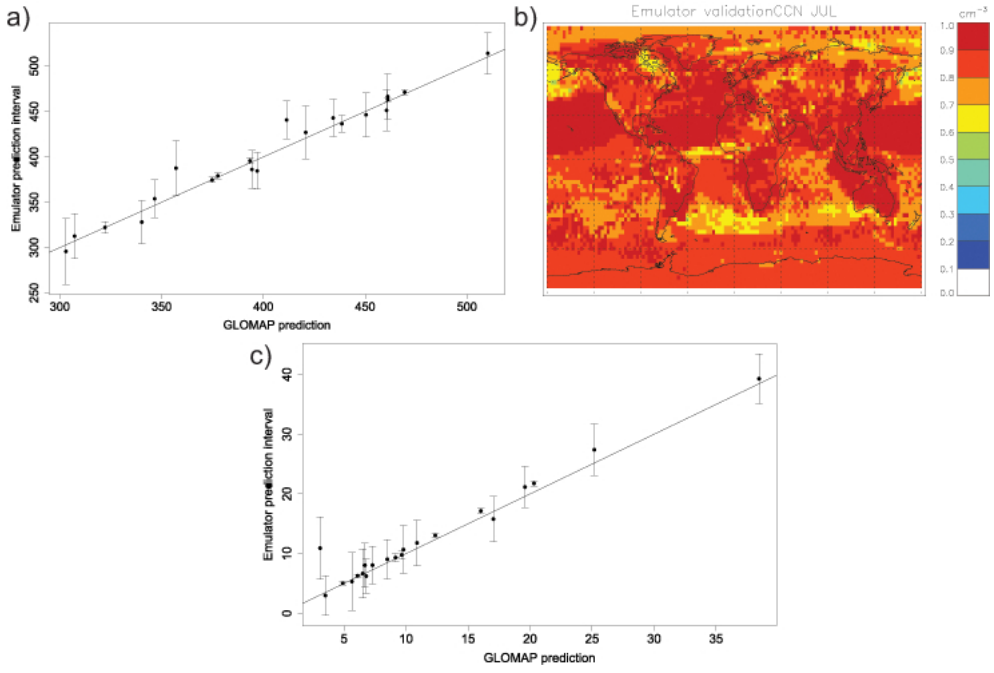

Fig. 1. Validation of the emulators. **(a)** shows the emulator prediction versus the GLOMAP prediction in an example grid box **(b)** a summary of Figure a for every grid box calculated by counting the percentage of GLOMAP predictions lying in the emulator prediction interval **(c)** an example grid box where the emulator does predict closely to the GLOMAP prediction but with so much confidence the GLOMAP prediction does not lie in the emulator prediction interval.

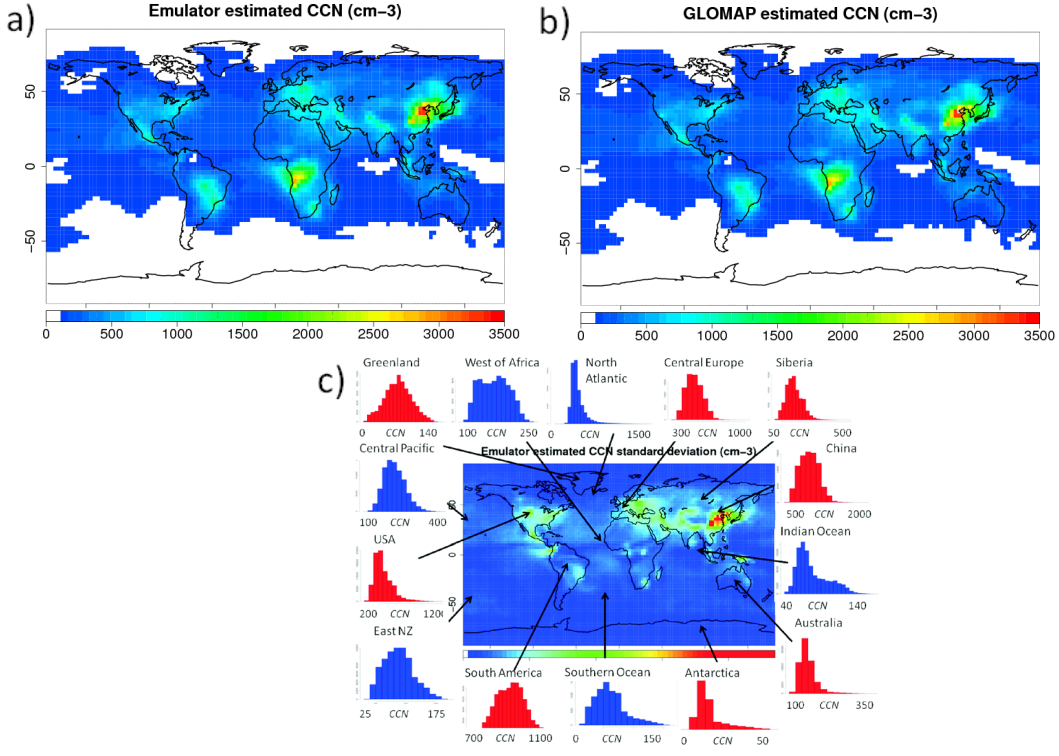

Fig. 2. Estimated July 2000 CCN from **(a)** the emulator and **(b)** the mean CCN from the 80 GLOMAP-mode runs. Panel **(c)** shows the uncertainty in the CCN (calculated as the standard deviation from the emulator) with posterior CCN distributions from the 80 000 emulator simulations shown for 13 locations.

Table 1. The model parameters and emissions, and their uncertainty ranges, used in this study.

Number	Short name	Parameter	Description	Uncertainty limits
X1	OX_DIAM	Oxidation activation diameter	Activation of aerosol to cloud droplets in stratiform clouds	[40,125] nm
X2	ACC_COEF	Mass accommodation coefficient	Probability that a molecule of H_2SO_4 sticks to aerosol on collision	[0.02–1.00]
X3	NUC_THRESH	H_2SO_4 nucleation threshold	Threshold concentration for new particles to be formed	[0.25–4.0] × baseline
X4	NUCRIT_SIZE	Nucleation critical cluster size	Smallest size above which a H_2SO_4 cluster is stable	[50–100] molecules
X5	SO2_PART	Sulphate particulate emissions	% of sulphur emissions in each gridbox set to particulate	0–5 % of SO_2
X6	SCAV_DIAM	Cloud nucleation scavenging diameter	Threshold for aerosol that can grow to rain droplets to be scavenged	[80–250] nm
X7	SO2_EMS	Sulphur emissions	Factor describing uncertainty in emissions inventory	70–130 % baseline
X8	SS_EMS	Sea spray emissions	Factor describing uncertainty in derived sea spray emissions	0.1–10 × baseline

Table 2. The uncertainty around the emulator estimated CCN due to emulation and due to the uncertain parameters at 14 grid boxes shown in Fig. 2

Grid box location	Uncertainty due to emulation, $\hat{V}^*(E)$	Uncertainty due to the 8 uncertain parameters, $\hat{E}^*(V)$
North Atlantic	0.5	522
Central Europe	4.8	6378
Siberia	2.8	2499
China	32.8	34 977
Indian Ocean	0.15	383
Australia	0.9	792
Antarctica	0.03	78.1
Southern Ocean	0.1	673
South America	3.7	4178
East of New Zealand	0.39	628
USA	11.2	14 076
Central Pacific	2.3	1906
Greenland	0.2	309
West of Africa	0.1	921

shows posterior CCN distributions for 13 locations, illustrating that the emulator does not necessarily produce symmetric CCN distributions, even though the input parameter uncertainties were uniform. A range of distributional shapes can be seen, with remote regions having strongly skewed pdf, with a long tail of low probability high CCN concentrations. These posterior CCN distributions were produced by sampling 80 000 points from the emulator mean function and not from the 80 model simulations. Although 80 simulations sounds a lot, it is actually far less than is required to generate statistically reliable probability distributions or to perform a full variance-based sensitivity analysis, as we are able to do in the next section using an emulator. The number of runs typically required to produce statistically reliable results is discussed in O'Hagan (2006) and the number of runs required to produce the sensitivity measures with the extended-FAST method is discussed in Cukier et al. (1977).

The highest CCN concentrations over polluted areas correlate with the regions of highest absolute uncertainty. However, relative changes in CCN are more relevant for changes in cloud albedo and climate than absolute concentrations (Twomey, 1991). In fact, changes in albedo are more sensitive to changes in CCN when concentrations are low, thus the absolute variance map will give a misleading impression of the importance of the uncertainty. To understand the relative uncertainty in CCN we define the coefficient of variation as $\sigma_{\mathrm{CCN}_{ij}}/\mu_{\mathrm{CCN}_{ij}}$ with $\mu_{\mathrm{CCN}_{ij}}$ and $\sigma_{\mathrm{CCN}_{ij}}$ calculated using the emulator for every grid box ij. In contrast, the coefficient of variation (Fig. 3) shows the opposite pattern, with the highest values over remote regions. The coefficient of variation reaches a maximum at high latitudes where the uncertainty is 50–80 % of the CCN concentration. The apparent very low CCN uncertainty over South Africa and South

America is likely only due to those regions being dominated by biomass burning emissions parameters, which were not included in the 8 chosen parameters here. A future study will cover a much more complete set of uncertain model parameters, with expert elicitation used to ensure all important processes are considered.

4.3 CCN sensitivity to individual parameters

To identify which parameter uncertainties contribute to the CCN uncertainty in each region, we carry out sensitivity analysis to quantify the relative contribution of each of the parameter uncertainties to the overall CCN uncertainty in Fig. 1. Sensitivity analysis is carried out for each model grid box based on a separate emulator. The main effect contributions of each parameter to the CCN variance are shown in Fig. 4 and the corresponding absolute standard deviation in Fig. 5. Figure 4 shows the relative importance of uncertainty in different processes in different global regions. Note that the effect of a given parameter on the CCN uncertainty in any grid box does not imply that the process is localised to that grid box. The aerosol in any location has undergone long-range transport and transformation, so the parameter sensitivity in a given grid box depends on the integrated effect of the uncertain parameter over the lifecycle of the aerosol during transport.

The main contributors to CCN uncertainty in the Southern Ocean and polar regions are uncertainty in the scavenging diameter (the size above which particles are assumed to be nucleation scavenged in precipitating gridboxes) and the sea spray emissions, which account for over 60 % of the variance throughout these regions. These are also the regions with the greatest coefficient of variation (Fig. 3). The areas of highest uncertainty in CCN in Fig. 2 are dominated by the ± 30 % uncertainty in the SO_2 emissions, which accounts for over 70 % of the variance in regions dominated by anthropogenic sulphur emissions. Two of the chosen parameters, the nucleation critical cluster size and the fraction of anthropogenic SO_2 emissions to be emitted in particulate form, lead to < 10 % of the variance in CCN concentrations and are hence considered insensitive, Fig. 5 shows that the absolute standard deviation in CCN from uncertainty in these two parameters is also small. The lack of sensitivity to subgrid particulate SO_4 emissions is surprising as previous work has shown sensitivity to this parameter (Adams and Seinfeld, 2003). However, in these simulations we followed Stier et al. (2005) and emitted at a larger size than Adams and Seinfeld (2003), thus the sensitivity is much less. In the next experiment, the size, as well as the emission rate, of the particulates will be investigated based on new information from detailed plume studies (Stevens et al., 2012).

The mid tropical oceans are dominated by uncertainty in the oxidation activation diameter (the size above which soluble particles are assumed to activate to cloud droplets in stratiform cloud), which accounts for nearly 90 % of the variance

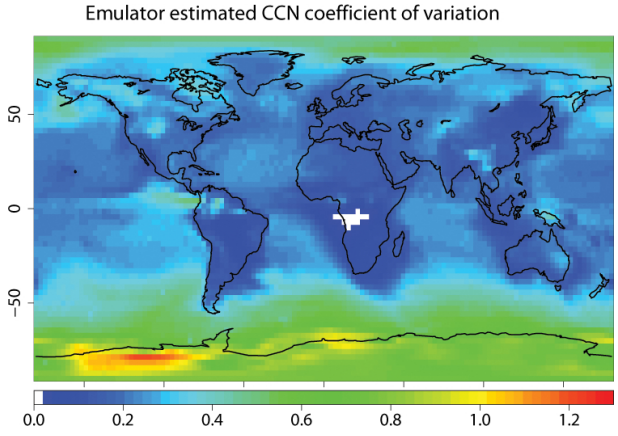

Fig. 3. The CCN coefficient of variation ($\sigma_{\mathrm{CCN}_{ij}}/\mu_{\mathrm{CCN}_{ij}}$ for gridbox ij) shows how well constrained the July 2000 CCN is in each gridbox with respect to the uncertainty in the 8 parameters in Table 1.

in this region. The absolute standard deviation contribution map (Fig. 5) shows that this process is most important over the regions of persistent marine stratocumulus clouds (e.g., off the west coast of Namibia and Central America).

Whereas in polluted regions, the CCN uncertainty is mainly from SO_2 emissions, in less-polluted continental regions, CCN are more sensitive to the uncertainties in the accommodation coefficient and nucleation threshold, which have a similar spatial pattern. The nucleation threshold controls nucleation of sulphuric acid particles in the free troposphere (FT) (Kulmala et al. (1998); Spracklen (2005)). Merikanto et al. (2009) showed that FT nucleation is a significant source of CCN to the boundary layer (the altitude that we analyse here). The impact of this nucleation on boundary layer CCN depends on the growth of the nuclei to CCN sizes during downward transport and mixing, which is mainly driven by sulphuric acid condensation, hence the mass accommodation coefficient (ACC_COEF in Fig. 4). The result is consistent with Merikanto et al. (2009) where it was shown that the FT CCN source is amplified over land areas because the particles grow more rapidly due to uptake of the available biogenic SOA and anthropogenic sulphuric acid over polluted continental regions.

It is important to distinguish between the importance of a parameter in controlling the mean CCN concentration and its importance in controlling the uncertainty in CCN. A process or emission has to make a significant contribution to CCN for the CCN to be sensitive to parameters controlling that process, but the converse is not necessarily true. The nucleation threshold seems to be a parameter that behaves like this. In Merikanto et al. (2009) we showed that FT nucleation is a major source of boundary layer CCN, accounting for up to 80 % of CCN over some marine regions. However, in Fig. 4, NUC_THRESH contributes to CCN variance mainly over land areas. A plausible explanation is that over marine

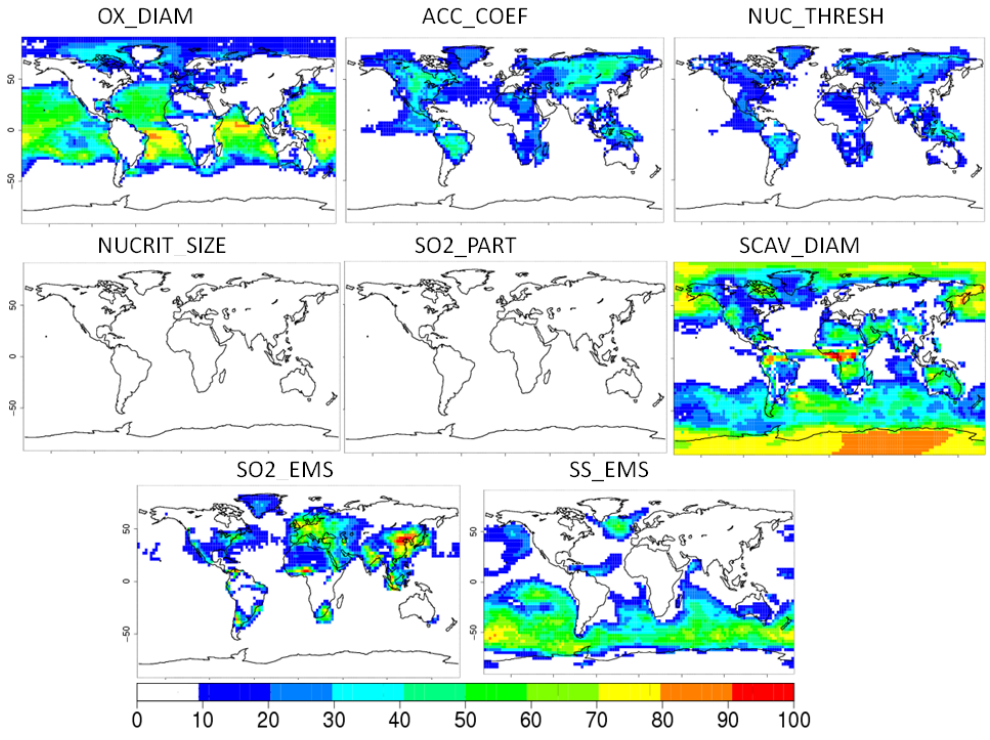

Fig. 4. Percentage of July 2000 CCN variance due to uncertainty in each of the 8 parameters in Table 1 – the main effect.

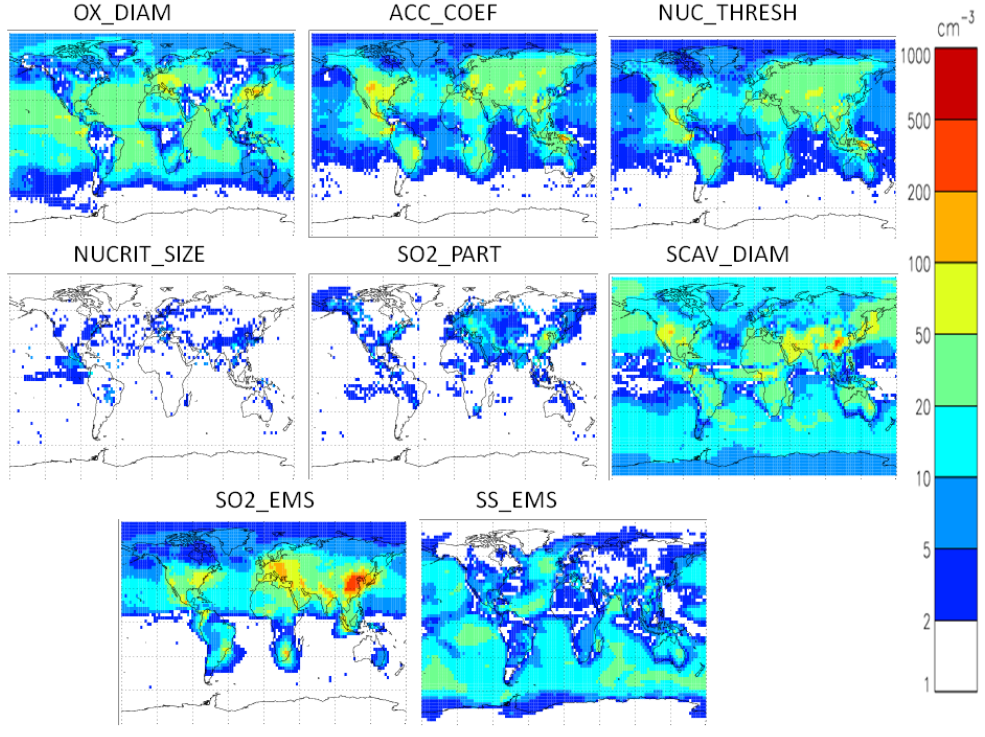

Fig. 5. The absolute July 2000 CCN standard deviation due to uncertainty in each of the 8 parameters in Table 1. The absolute standard deviation compared to the most sensitive parameters can help modellers choose which of the parameters is most important in the attempt to reduce uncertainty in global CCN modelling.

regions there is very little condensable vapour to grow the nuclei to CCN sizes, so growth is mainly through coagulation, which reduces particle concentrations and reduces the sensitivity to the initial nucleation rate, a result that is predicted theoretically Clement and Ford (1999). Thus, FT nucleation makes a large contribution to mean boundary layer CCN concentrations over marine regions, but the concentration is not very sensitive to the nucleation rate in the free and upper troposphere.

4.4 Parameter interactions

By using the emulation approach we are able to investigate the entire parameter uncertainty space and therefore quantify the interactions between the 8 uncertain parameters shown. Interactions indicate non-linear coupling of parameter effects in the GLOMAP output. For example, if the total effect variance is equal to the main effect for a given parameter, then that parameter impacts CCN independently of the other parameters and a one-at-a-time test will be sufficient to determine the total sensitivity. Interactions occur when, for example, a high setting of one parameter amplifies or suppresses the sensitivity to another parameter compared to its one-at-a-time sensitivity. Note, however, that the model response to one parameter can still be non-linear over its range even without interactions, but this single-parameter non-linearity is captured in our analysis as part of the main effect variance.

Figure 6 shows the percentage of the variance that is not caused by main effect of the parameters and is therefore caused by the interactions between the parameters; this is the percentage of the variance that cannot be quantified using OAT tests. Interactions are important in large regions of the globe including marine tropical regions (particularly in the Northern Hemisphere), Alaska, Siberia, Antarctica, Southernmost South America and South Australia. Interaction effects are negligible (and therefore OAT tests sufficient) over some of the more polluted regions such as Europe and East China. The peak contribution of interaction effects to the total variance is about 50 %, thus OAT tests would underestimate the uncertainty in CCN in these regions by this amount.

The contributions of each parameter to the interaction effect are shown in Fig. 7. These were calculated by subtracting the main effect from the total effect for each parameter. By examining the spatial patterns of the interactions it is possible to determine which parameters interact with each other. The largest interaction is between the scavenging diameter and the oxidation activation diameter, which interact with each other or other model parameters throughout most of the globe and account for up to 30 % of the variance. These two parameters clearly account for CCN variance over Northern Hemisphere oceans, in the Arctic and over Alaska. Physically, this interaction can be explained by the effect of cloud processing on the aerosol size distribution, which impacts the scavenging in precipitating clouds. A low setting of the activation diameter in non-precipitating low clouds (the

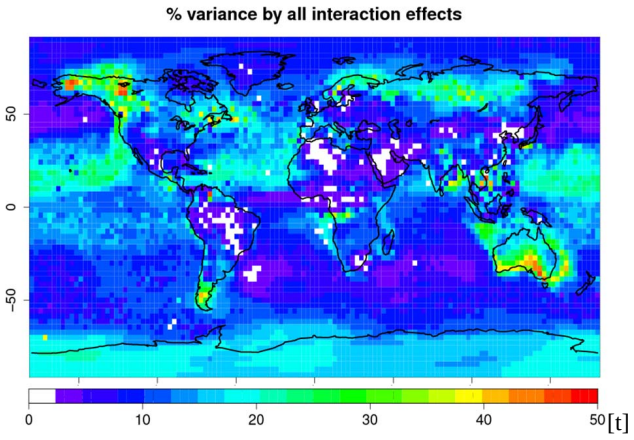

Fig. 6. Percentage of July 2000 CCN variance not explained by the main effect of the 8 parameters in Table 1. This is the variance explained by the interaction of the 8 parameter uncertainties and cannot be captured using OAT tests.

OX_DIAM parameter) leads to cloud processing and growth of a larger fraction of the aerosols, shifting the size distribution to sizes where scavenging can occur in precipitating clouds.

Another strong interaction occurs between sea spray emissions and the scavenging diameter, which is apparent over Southern Australia, Southernmost South America and Antarctica. This large interaction is due to the diminishing sensitivity of the scavenging diameter as the sea spray emissions increase. The other dominant interaction is between the accommodation coefficient of sulphuric acid (ACC_COEF) and the binary homogeneous nucleation threshold (NUC_THRESH). This interaction accounts for up to 30 % of the variance over the Northern Hemisphere land areas. Sulphur emissions do not interact with the other processes considered in this study thus could be investigated using OAT tests.

4.5 Identification of dominant parameters

An understanding of the important processes that control the uncertainty in CCN can help to direct research efforts to the processes of most global importance. Learning the global importance of each parameter and the CCN uncertainty that it contributes means that the value of future research can be quantified.

Figure 8 shows maps of the dominant parameter (of the 8) leading to uncertainty in the CCN concentration and the fraction of CCN variance explained by its total effect (the effect of the parameter individually and all its interactions). The uncertainty in oxidation diameter dominates in 35 % of the boundary layer, scavenging diameter uncertainty dominates in 28 % and sea spray dominates uncertainty in 17 % of the boundary layer. Five parameters are the dominant uncertainty in less than 10 % of the boundary layer. There

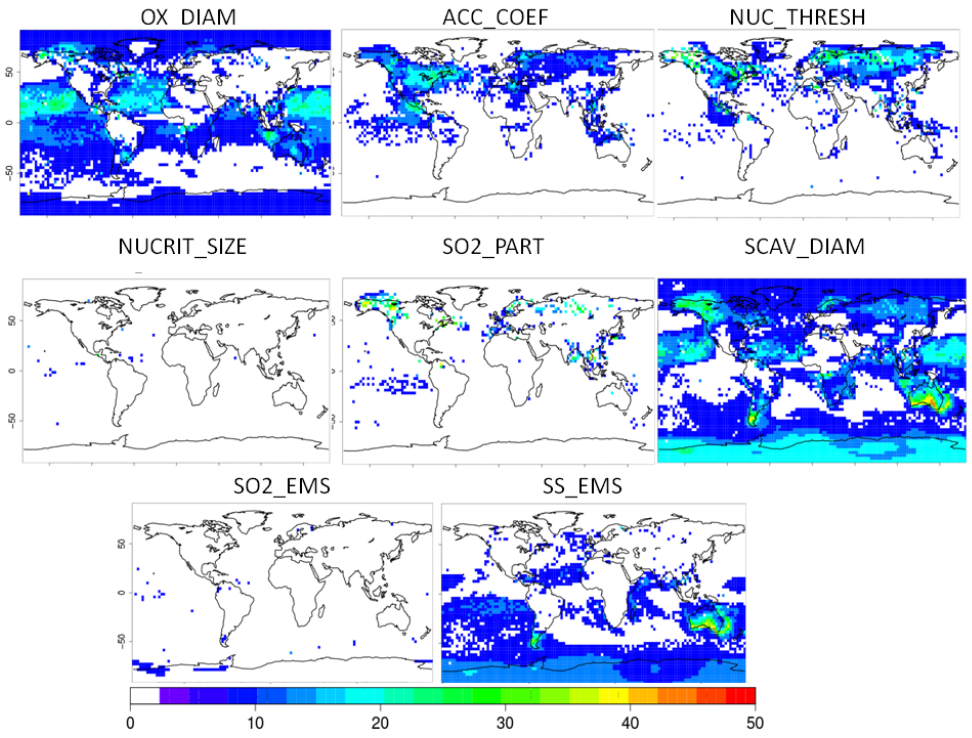

Fig. 7. The interaction effect of the individual parameters in Table 1 on July 2000 CCN uncertainty (calculated by the total effect minus the main effect).

is large variation in the fraction of variance explained by the dominant parameter. The simplest regions are dominated by one parameter (scavenging diameter) that controls 70–90 % of the variance in the remote marine regions and > 90 % of the variance in Antarctica. Thus, the CCN variance in July would be reduced by 70–90 % if this parameter could be learnt precisely. It may not always be possible to learn a parameter precisely, in which case this is the uncertainty that is irreducible if the representation of a process cannot be improved. There are other regions where only 20–40 % of the variance is explained by the dominant parameter. Over most land areas the dominant parameter accounts for 40 % of the CCN variance, suggesting the variance is shared between multiple parameters, as can be seen in Fig. 4. The mid-tropical oceans are dominated by uncertainty in the oxidation activation diameter which accounts for between 40 and 100 % of the variance but the CCN concentration in this region is reasonably well constrained, with a coefficient of variation of only 0.2–0.3 (Fig. 3).

5 Conclusions

Emulation is a powerful method for understanding the sources of uncertainty in a complex global model. It is based on well established statistical theory with clear prior assumptions as detailed in Sect. 3. The choice of priors used in GP emulation can be tested with no further model runs to test for statistical robustness. A relatively small number of model simulations covering the uncertainty space of the parameters generates sufficient information to enable a full variance-based sensitivity analysis to be performed, which would otherwise require an unfeasibly large number of model simulations using a Monte Carlo approach. The emulator is computationally efficient and can therefore be built for every grid box of a global model. Here we have focused on CCN, but similar information could be generated for optical depth or any other quantity based on the existing model runs. The emulator also generates a full probability density function (pdf) of any model output in every grid box, which is not constrained to be Gaussian. Compared to one-at-a-time sensitivity tests the emulator generates vastly more information to aid model development and uncertainty reduction.

Our results show that variance-based analysis of the emulated global model produces spatial patterns of parameter dependencies and interactions that make sense in terms of the processes that control the properties of the aerosol in different regions. There is a high degree of coherence in the patterns, suggesting that the variance analysis is generating physically meaningful information about the response of the model to its uncertain parameters. The spatial distribution of the variance contribution of some parameters is clearly localised to the place where that parameter is acting. For example, the uncertainty in sea spray emissions shows up primarily in windy marine regions. However, the uncertainty

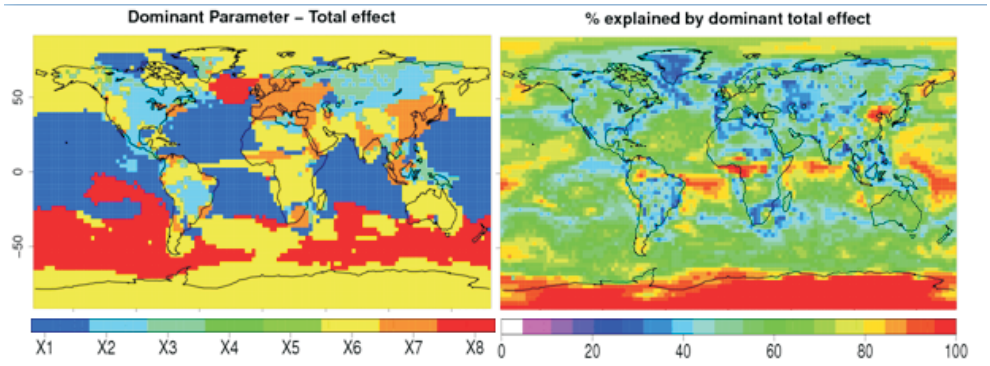

Fig. 8. The dominating total effect in each model gridbox and the percentage of July 2000 CCN variance explained by it.

in some parameters has a non-local impact on CCN variance. For example, aerosol wet scavenging strongly affects the overall CCN uncertainty in remote non-cloudy regions and the interaction of uncertain sea spray emissions with other parameters influences CCN over Antarctica.

Our approach, which could readily be extended to a larger set of parameters and eventually more models, provides a framework for the quantifiable reduction in model uncertainty and improvement in robustness. A robust model is one that is still reliable when its uncertain parameters are varied. However, robustness cannot be assessed from a very limited set of one-at-a-time parameter perturbations. Model evaluation based on comparing the full pdf of model results against observations will enable model robustness to be tested for the first time. Emulation of observable quantities such as CCN, particle concentrations and aerosol optical depth will allow the comparison of emulated values to observations, leading to a reduction in the parametric uncertainty by constraining the model output space. The results can be used to understand where parameter uncertainty is reducible and where it is irreducible.

A complete understanding of the model behaviour within the parameter uncertainties will also aid the next step of reducing model uncertainty: calibration. Calibration, which is widely used in other fields of environmental modelling, is the identification of the model that best matches observations within defined criteria (e.g., of bias, correlation, etc.) (Kennedy and O'Hagan, 2001). Aerosol model calibration would be a significant step compared to previous studies that have attempted to identify the best model based on a very small number of model sensitivity tests. In such cases we have no idea whether poor model performance is simply due to neglect of a plausible part of the parameter space, which can now be fully quantified using the emulator.

Our approach could also provide a way to more reliably identify model structural weaknesses and thereby prioritise future model development. Structural weaknesses will become apparent by identifying regions (e.g., free troposphere, Arctic) or conditions (clean, polluted, cloudy) where the model-observation bias is outside the full range of parameter uncertainties (defined by the pdf). Such discrepancies will either indicate that we have not considered all the important parameters (or underestimated their uncertainty range) of the present model or that the model has structural deficiencies such as neglected emissions, incomplete processes or deficiencies in the host transport model.

Global analyses of uncertainty sources could also be used to develop new measurement strategies to maximise the reduction in uncertainty in aerosol forcing. Variance maps can be used to define the location and type of measurements that will have the greatest impact on reducing uncertainty in CCN or any other aerosol quantity. At present, many field campaigns make novel measurements of unexplored aerosol properties and processes but are less steered by the requirement to develop more robust models. To extend this work to aerosol forcing the results of the GLOMAP runs can be directly fed into radiative code and the corresponding radiative effect quantities obtained. The emulators can then be built with the radiative effect quantities rather than the CCN, following the same method.

A further extension of the model emulation approach will be to study the importance of interactions, for example in the air quality-climate system. Most mitigation studies focus on the response of atmospheric composition or climate to one parameter at a time (e.g., SO_2 or NO_x emission reductions), although future air quality and climate will be driven by simultaneous changes in many parameters. The emulator results that we have analysed here to quantify variance can also be used to understand the model response surface. This will enable the response of, say, particulate matter, to all possible combinations of emissions changes to be investigated based on a relatively small number of model simulations.

Acknowledgements. We acknowledge funding from the Natural Environment Research Council AEROS project under grant NE/G006172/1 and the EU FP7 IP PEGASOS (FP7-ENV-2010/265148).

Edited by: E. Nemitz

References

Ackerley, D., Highwood, E., Frame, D., and Booth, B.: Changes in the global sulfate burden due to perturbations in global CO_2 concentrations, J. Climate, 20, 5421–5432, 2009.

Adams, P. J. and Seinfeld, J. H.: Disproportionate impact of particulate emissions on global cloud condensation nuclei concentrations, Geophys. Res. Lett., 30, 1239, doi:10.1029/2002GL016303, 2003.

Carnell, R.: lhs: Latin Hypercube Samples, available at: http://CRAN.R-project.org/package=lhs, r package version 0.5, last access: 15 December 2011, 2008.

Chipperfield, M.: New version of the TOMCAT/SLIMCAT offline chemical transport model: intercomparison of stratospheric tracer experiments, Q. J. Roy. Meteorol. Soc., 132, 1179–1203, doi:10.1256/qj.05.51, 2006.

Clement, C. F. and Ford, I. J.: Gas-to-particle conversion in the atmosphere: II. Analytical models of nucleation bursts, Atmos. Environ., 33, 489–499, 1999.

Cukier, R. I., Levine, H. B., and Shuler, K. E.: Nonlinear sensitivity analysis of multiparameter model systems, J. Phys. Chem., 81, 2365–2366, 1977.

Forster, P., Ramaswamy, V., Artaxo, P., Berntsen, T., Betts, R., Fahey, D., Haywood, J., Lean, J., Lowe, D., Myhre, G., Nganga, J., Prinn, R., Raga, G., Schulz, M., and Van Dorland, R.: Changes in atmospheric constituents and in radiative forcing, in: Climate Change 2007: The Physical Science Basis. Contribution of Working Group I to the Fourth Assessment Report of the Intergovernmental Panel on Climate Change, edited by: Solomon, S., Qin, D., Manning, M., Chen, Z., Marquis, M., Averyt, K. B., Tignor, M., and Miller, H. L., Cambridge University Press, Cambridge, UK and New York, NY, USA, 2007.

Haerter, J. O., Roeckner, E., Tomassini, L., and von Storch J.-S.: Parametric uncertainty effects on aerosol radiative forcing, Geophys. Res. Lett., 36, L15707, doi:10.1029/2009GL039050, 2009.

Kennedy, M.: The GEM software project, available at: http://www.ctcd.group.shef.ac.uk/gem.html, Centre for Terrestrial Carbon Dynamics (CTCD), 2004.

Kennedy, M. and O'Hagan, A.: Bayesian calibration of computer models (with discussion), J. Roy. Stat. Soc. B Met., 63, 425–464, 2001.

Kulmala, M., Laaksonen, A., and Pirjola, L.: Parameterizations for sulfuric acid/water nucleation rates, J. Geophys. Res., 103, 8301–8307, 1998.

Lee, L. A., Carslaw, K. S., Pringle, K. J., Mann, G. W., and Spracklen, D. V.: Emulation of a complex global aerosol model to quantify sensitivity to uncertain parameters, Atmos. Chem. Phys., 11, 12253–12273, doi:10.5194/acp-11-12253-2011, 2011.

Lohmann, U. and Ferrachat, S.: Impact of parametric uncertainties on the present-day climate and on the anthropogenic aerosol effect, Atmos. Chem. Phys., 10, 11373–11383, doi:10.5194/acp-10-11373-2010, 2010.

Mann, G. W., Carslaw, K. S., Spracklen, D. V., Ridley, D. A., Manktelow, P. T., Chipperfield, M. P., Pickering, S. J., and Johnson, C. E.: Description and evaluation of GLOMAP-mode: a modal global aerosol microphysics model for the UKCA composition-climate model, Geosci. Model Dev., 3, 519–551, doi:10.5194/gmd-3-519-2010, 2010.

Mann, G. W., Carslaw, K. S., Ridley, D. A., Spracklen, D. V., Pringle, K. J., Merikanto, J., Korhonen, H., Schwarz, J. P., Lee, L. A., Manktelow, P. T., Woodhouse, M. T., Schmidt, A., Breider, T. J., Emmerson, K. M., Reddington, C. L., Chipperfield, M. P., and Pickering, S. J.: Intercomparison of modal and sectional aerosol microphysics representations within the same 3-D global chemical transport model, Atmos. Chem. Phys., 12, 4449–4476, doi:10.5194/acp-12-4449-2012, 2012.

McKay, M., Conover, W., and Beckman, R.: A comparison of three methods for selecting values of input variables in the analysis of output from a computer code, Technometrics, 21, 239–245, 1979.

Meehl, G. A., Covey, C., Delworth, T., Latif, M., McAvaney, B., Mitchell, J., Stouffer, R., and Taylor, K.: The WCRP CMIP3 multi-model dataset: a new era in climate change research, B. Am. Meteorol. Soc., 88, 1383–1394, 2007.

Merikanto, J., Spracklen, D. V., Mann, G. W., Pickering, S. J., and Carslaw, K. S.: Impact of nucleation on global CCN, Atmos. Chem. Phys., 9, 8601–8616, doi:10.5194/acp-9-8601-2009, 2009.

O'Hagan, A.: Bayesian analysis of computer code outputs: a tutorial, Reliab. Eng. Syst. Safe., 91, 1290–1300, 2006.

Pan, W., Tatang, M., McRae, G., and Prinn, R.: Uncertainty analysis of direct radiative forcing by anthropogenic sulfate aerosols, J. Geophys. Res., 102, 21915–21924, 1997.

Partridge, D. G., Vrugt, J. A., Tunved, P., Ekman, A. M. L., Struthers, H., and Sorooshian, A.: Inverse modelling of cloud-aerosol interactions – Part 2: Sensitivity tests on liquid phase clouds using a Markov chain Monte Carlo based simulation approach, Atmos. Chem. Phys., 12, 2823–2847, doi:10.5194/acp-12-2823-2012, 2012.

Penner, J., Andreae, M., Annegarn, H., Barrie, L., Feichter, J., Hegg, D., Jayaraman, A., Leaitch, R., Murphy, D., Nganga, J., and Pitar, G.: Aerosols, their direct and indirect effects, in: Climate Change 2001: The Scientific Basis. Contribution of Working Group I to the Third Assessment Report of the Intergovernmental Panel on Climate Change, edited by: Houghton, J. T., Ding, Y., Griggs, D. J., Noguer, M., van der Linden, P. J., Dai, X., Maskell, K., and Johnson, C. A., Cambridge University Press, Cambridge, UK and New York, NY, USA, 2001.

Pujol, G.: Sensitivity: sensitivity analysis, available at: http://CRAN.R-project.org/package=sensitivity, r package version 1.4-0, last access: 15 December 2011, 2008.

Roustant, O., Ginsbourger, D., and Deville, Y.: DiceKriging: kriging methods for computer experiments, available at: http://CRAN.R-project.org/package=DiceKriging, r package version 1.3.2, last access: 15 December 2011, 2011.

Saltelli, A. and Annonia, P.: How to avoid a perfunctory sensitivity analysis, Environ. Modell. Softw., 25, 1508–1517, 2010.

Saltelli, A., Tarantola, S., and Chan, K. P.-S.: A quantitative model-independent method for global sensitivity analysis of model output, Technometrics, 41, 39–56, doi:10.2307/1270993, 1999.

Schimel, D., Alves, D., Enting, I., Heimann, M., Joos, F., Raynaud, D., Wigley, T., Prather, M., Derwent, R., Ehhalt, D., Fraser, P., Sanhueza, E., Zhou, X., Jonas, P., Charlson, R., Rodhe, H., Sadasivan, S., Shine, K., Fouquart, Y., Ramaswamy, V., Solomon, S., Srinivasan, J., Albritton, D., Derwent, R., Isaksen, I., Lal, M., and Wuebbles, D.: Radiative forcing of climate change, in: Climate Change 1996, Contribution of Working Group I to the 2nd Assessment Report of the Intergovernmental Panel on Climate Change, edited by: Houghton, J. T.,

Meira Filho, L. G., Callander, B. A., Harris, N., Kattenberg, A., and Maskell, K., Cambridge University Press, Cambridge, UK and New York, NY, USA, 1996.

Spracklen, D. V.: Development and application of a Glomap Model of Aerosol Processes (GLOMAP), Ph.D. thesis, University of Leeds, UK, 2005.

Spracklen, D. V., Pringle, K. J., Carslaw, K. S., Chipperfield, M. P., and Mann, G. W.: A global off-line model of size-resolved aerosol microphysics: II. Identification of key uncertainties, Atmos. Chem. Phys., 5, 3233–3250, doi:10.5194/acp-5-3233-2005, 2005.

Spracklen, D. V., Carslaw, K. S., Merikanto, J., Mann, G. W., Reddington, C. L., Pickering, S., Ogren, J. A., Andrews, E., Baltensperger, U., Weingartner, E., Boy, M., Kulmala, M., Laakso, L., Lihavainen, H., Kivekäs, N., Komppula, M., Mihalopoulos, N., Kouvarakis, G., Jennings, S. G., O'Dowd, C., Birmili, W., Wiedensohler, A., Weller, R., Gras, J., Laj, P., Sellegri, K., Bonn, B., Krejci, R., Laaksonen, A., Hamed, A., Minikin, A., Harrison, R. M., Talbot, R., and Sun, J.: Explaining global surface aerosol number concentrations in terms of primary emissions and particle formation, Atmos. Chem. Phys., 10, 4775–4793, doi:10.5194/acp-10-4775-2010, 2010.

Stevens, R. G., Pierce, J. R., Brock, C. A., Reed, M. K., Crawford, J. H., Holloway, J. S., Ryerson, T. B., Huey, L. G., and Nowak, J. B.: Nucleation and growth of sulfate aerosol in coal-fired power plant plumes: sensitivity to background aerosol and meteorology, Atmos. Chem. Phys., 12, 189–206, doi:10.5194/acp-12-189-2012, 2012.

Stier, P., Feichter, J., Kinne, S., Kloster, S., Vignati, E., Wilson, J., Ganzeveld, L., Tegen, I., Werner, M., Balkanski, Y., Schulz, M., Boucher, O., Minikin, A., and Petzold, A.: The aerosol-climate model ECHAM5-HAM, Atmos. Chem. Phys., 5, 1125–1156, doi:10.5194/acp-5-1125-2005, 2005.

Textor, C., Schulz, M., Guibert, S., Kinne, S., Balkanski, Y., Bauer, S., Berntsen, T., Berglen, T., Boucher, O., Chin, M., Dentener, F., Diehl, T., Easter, R., Feichter, H., Fillmore, D., Ghan, S., Ginoux, P., Gong, S., Grini, A., Hendricks, J., Horowitz, L., Huang, P., Isaksen, I., Iversen, I., Kloster, S., Koch, D., Kirkevåg, A., Kristjansson, J. E., Krol, M., Lauer, A., Lamarque, J. F., Liu, X., Montanaro, V., Myhre, G., Penner, J., Pitari, G., Reddy, S., Seland, Ø., Stier, P., Takemura, T., and Tie, X.: Analysis and quantification of the diversities of aerosol life cycles within AeroCom, Atmos. Chem. Phys., 6, 1777–1813, doi:10.5194/acp-6-1777-2006, 2006.

Textor, C., Schulz, M., Guibert, S., Kinne, S., Balkanski, Y., Bauer, S., Berntsen, T., Berglen, T., Boucher, O., Chin, M., Dentener, F., Diehl, T., Feichter, J., Fillmore, D., Ginoux, P., Gong, S., Grini, A., Hendricks, J., Horowitz, L., Huang, P., Isaksen, I. S. A., Iversen, T., Kloster, S., Koch, D., Kirkevåg, A., Kristjansson, J. E., Krol, M., Lauer, A., Lamarque, J. F., Liu, X., Montanaro, V., Myhre, G., Penner, J. E., Pitari, G., Reddy, M. S., Seland, Ø., Stier, P., Takemura, T., and Tie, X.: The effect of harmonized emissions on aerosol properties in global models – an AeroCom experiment, Atmos. Chem. Phys., 7, 4489–4501, doi:10.5194/acp-7-4489-2007, 2007.

Twomey, S.: Aerosols, clouds and radiation, Atmos. Environ. Part A., 25, 2435–2442, doi:10.1016/0960-1686(91)90159-5, 1991.